Check for updates

Comparative Analysis of Heat Release, Bound Water Content and Compressive Strength of Alkali-Activated Slag-Fly Ash

Shiju Joseph and Özlem Cizer*

Civil Engineering Department, KU Leuven, Leuven, Belgium

Optimizing the mix composition of alkali-activated materials is sometimes overwhelming due to the higher number of potential parameters that could be varied compared to designing a mix based on Portland cement. The present work focuses on understanding the correlations between compressive strength, bound water content, and heat release from the calorimeter. Different slag and fly ash proportions are studied at two different solution-to-binder (S/B) ratios. Alkali solutions are made with 5 M NaOH and water glass to have a final silica modulus of 1.28. Results indicate that, at similar S/B ratios, mixes with high amounts of slag develop high compressive strength corresponding to high bound water contents until 28 days and high heat release until 7 days. A good correlation exists between compressive strength with cumulative heat release and bound water content when the water-to-solid ratio of the initial mixture is also considered. These findings promise a less tedious method that could be employed to optimize the process for the mix design of alkali-activated materials.

Keywords: alkali-activation, blast furnace slag, fly ash, heat release, bound water, strength

INTRODUCTION

Portland cement has been the standard binder in the global use of concrete in construction for more than a century. As a result, cement production contributes to a large share of manmade emissions and environmental footprint due to the massive volumes of concrete production worldwide. One of the many possible routes (Juenger et al., 2011) to reduce its detrimental impact is the use of alkali-activated materials (AAMs) in concrete with desired engineering and durability performance in specific applications (Roy, 1999; Provis and Deventer, 2014; Pachego-Torgal et al., 2015; Provis, 2018). This class of binders, studied considerably in the past decades, generally uses supplementary cementitious materials (SCMs) as precursors. These SCMs are mostly industrial by-products such as blast furnace slag and coal combustion fly ashes. While several other possible SCMs are available, the sheer quantity available on a global scale (Snellings, 2016) and the significant amount of research conducted on these materials make these two the most favorable choices for AAM. SCMs are hardly reactive while mixed with water. Hence, strong alkalis such as sodium hydroxide (NaOH) and/or water glass (sodium silicates, $Na_2O.nSiO_2$) are needed for their activation as a binder.

Blends of blast furnace slag and fly ash have increased popularity that could complement each other. Blast furnace slag is highly reactive (Puligilla and Mondal, 2013), and fly ash can greatly improve the workability of the mixes owing to its spherical morphology (Kutchko and Kim, 2006). It is often reported that blends with slag and fly ash provide better mechanical performance than with

TABLE 1 | Oxide composition of slag and fly ash.

| Materials	SiO_2	Al_2O_3	Fe_2O_3	CaO	MgO	SO_3	K_2O	Na_2O
Slag	36.2	12.4	0.6	39.8	7.3	—	0.5	—
Fly ash	54.5	26.5	6.6	3.5	2.0	1.3	2.9	1.0

FIGURE 1 | Particle size distribution.

blast furnace slag alone (Wardhono et al., 2015). Nevertheless, beyond a certain limit (typically 20%–35%), the replacement of slag with fly ash typically negatively affects the mechanical strength (Kumar et al., 2010).

One of the major criticisms of AAM on its ability to reduce the carbon footprint is the fact that they require large volumes of blast furnace slags to achieve comparable mechanical properties with Portland cements without high temperature curing at early ages. While almost all of the blast furnace slag produced globally is currently used to produce blended Portland cement, the carbon footprint cannot be solely reduced with this technology (Scrivener et al., 2018). In contrast, blast furnace slag usage in AAM further promotes the usage of other SCMs, which do not have sufficient reactivity to be used in Portland cement-based systems (Li et al., 2018; Skibsted and Snellings, 2019; Suraneni et al., 2019), which can be blended with slag to be efficiently activated with high concentration alkalis. Furthermore, there are many other niche applications where AAM could be more beneficial and efficient than Portland cement systems (Provis and Bernal, 2014; Luukkonen et al., 2019).

One of the major challenges in optimizing the mix composition of AAMs is the vast number of parameters that seriously impact the fresh and hardened properties. While the water-to-cement ratio (W/C) and temperatures are the major factors that govern the properties of Portland cement-based composites, AAMs are further dependent on the composition of the activators, including the type of the activating solution (e.g., NaOH, $Na_2O.nSiO_2$, Na_2SO_4, and Na_2CO_3), its molar concentration (which varies with the water-to-binder ratio), ratio of activators, and total amount of activators. Some studies have also investigated the possibility of improving the properties using additives such as reactive MgO and alkali activators (Jin et al., 2014; Fei et al., 2015).

Although recently more studies have focused on the usage of near-neutral activators (Rashad et al., 2013; Bernal, 2016; Mutti et al., 2020), sodium silicate-based activators are still more common because of the higher strength they impart. The composition of the sodium silicate solution has a considerable effect on the kinetics of the reaction. Increasing the silica modulus (Ms = SiO_2/Na_2O) without changing the Na_2O content increases the induction period, reduces the pH of the pore solution, reduces the early age strength, and typically increases the later age strength. The optimal composition of sodium silicate solution typically ranges from 0.75 to 1.5 Ms for maximum strength (Wang et al., 1994). The optimal total Na_2O content for maximum strength further depends on the slag and fly ash used as well (Marjanović et al., 2015).

Furthermore, as SCMs are generally waste products, their chemical and mineralogical composition often varies quite a
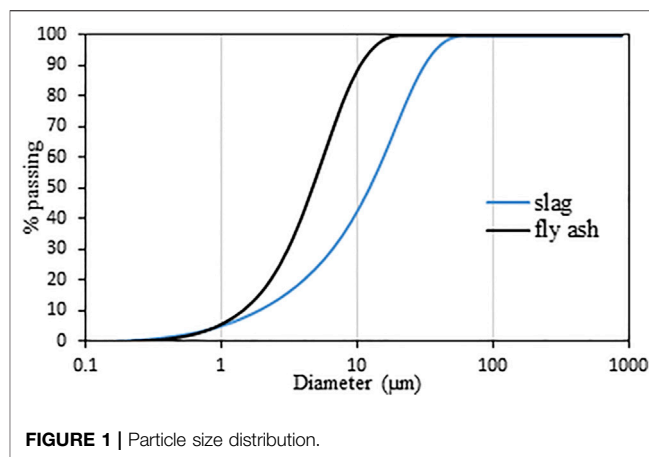
lot depending upon the source, and such changes in the composition of the precursors could alter the hydration products (Gong and White, 2016; Jin and Stephan, 2019). Furthermore, the fineness of the material, which significantly affects the kinetics of the reaction and the overall degree of hydration and strength development, mostly introduces another variability factor. Hence, the optimization challenge for these AAMs with respect to the fresh and hardened properties, also considering the economic point of view, is sometimes overwhelming and expensive.

This work aims to investigate the link between heat release, bound water content, and compressive strength so that the screening process, which needs to consider different factors, will be less tedious. In this work, heat release from isothermal calorimetry and bound water content determined from the thermogravimetric analysis is compared to the mortar compressive strength. The effects of different slag and fly ash ratios and solution-to-binder ratios are discussed.

EXPERIMENTAL PROTOCOL

The oxide compositions of the primary raw materials, ground granulated blast furnace slag, and coal combustion fly ash determined from X-ray fluorescence are reported in **Table 1**. The fineness of these materials determined using laser diffraction (Malvern Mastersizer 2000) is shown in **Figure 1** Alkali solutions were prepared using 99% pure sodium hydroxide pellets and sodium silicate solution (Na_2O 8.3%, SiO_2 27.5%). The activating solution of silica modulus (Ms) of 1.28 was prepared with 50% 5 M NaOH solution and 50% sodium silicate solution.

The different mixes used at various slag/fly ash ratios are tabulated in **Table 2**. Two sets of solution-to-binder ratios (S/B) were used, at a constant S/B ratio (of 0.7) and a varying S/B ratio, which give similar flow (~ 200 mm) for mortars prepared with river sand (0–2 mm) following the mixing protocol as described in EN 196–1. Although the fineness of fly ash is much higher compared to slag, the addition of fly ash considerably reduces the amount of solution required to achieve a similar flow. This should be attributed to the ball-bearing effect of the spherical fly ash

TABLE 2 | Mixes used in this work. S: solution; B: binder, w: water; s: solid.

Mix ID	Slag (%)	Fly ash (%)	S/B	Na$_2$O (% binder)	SiO$_2$ (% binder)	W/B	W/S
S100F0_0.7	100	0	0.7	7.5	9.6	0.52	0.44
S75F25_0.7	75	25	0.7	7.5	9.6	0.52	0.44
S50F50_0.7	50	50	0.7	7.5	9.6	0.52	0.44
S25F75_0.7	25	75	0.7	7.5	9.6	0.52	0.44
S0F100_0.7	0	100	0.7	7.5	9.6	0.52	0.44
S75F25_0.6	75	25	0.6	6.4	8.3	0.45	0.39
S50F50_0.55	50	50	0.55	5.9	7.6	0.42	0.36
S25F75_0.52	25	75	0.52	5.6	7.2	0.39	0.34
S0F100_0.49	0	100	0.49	5.3	6.7	0.37	0.32
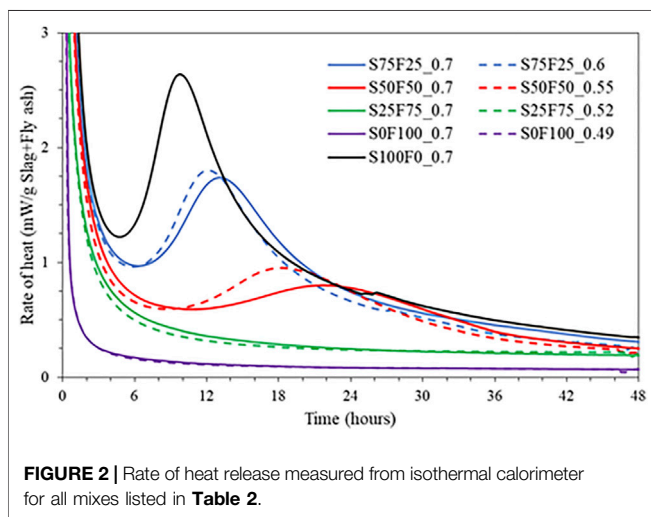
FIGURE 2 | Rate of heat release measured from isothermal calorimeter for all mixes listed in **Table 2**.

particles. All mix compositions were prepared at a fixed alkali modulus (SiO$_2$/Na$_2$O = 1.28).

The compressive strength for the different mixes listed in **Table 2** was measured on mortar beams following the protocols from EN 196–1. Compressive strength was measured at 3, 7, and 28 days for all mixes, and additional measurements at 90 days were carried out only for the mixes at an S/B ratio of 0.7. The heat release from pastes was recorded using TAM Air 8 channel isothermal calorimeter at 20°C for 7 days of hydration. The pastes were mixed in a temperature-controlled room at 20°C and then transferred to 20 ml ampules of the calorimeter. Therefore, the initial data of ~ 45 min after mixing are not considered in the data of cumulative heat release, including the initial ~ 15 min for mixing and placing in the calorimeter and the next 30 min measurement to achieve thermal stability in the calorimeter. Thermogravimetric analysis (TGA) was performed on pastes at 3, 7, and 28 days for all samples and at 90 days for samples with an S/B ratio of 0.7. TGA was carried out after hydration stoppage using a freeze dryer (0.025 mbar, –60°C, 2 h) without the initial pre-freezing with liquid nitrogen. Approximately 25–40 mg of ground samples (Joseph and Cizer, 2020) was used for thermogravimetric analysis (TGA) using NETZSCH STA 409 PC at a heating rate of 10°C/ min for a temperature range of 20°C–600°C with a nitrogen atmosphere (60 ml/min flow rate).
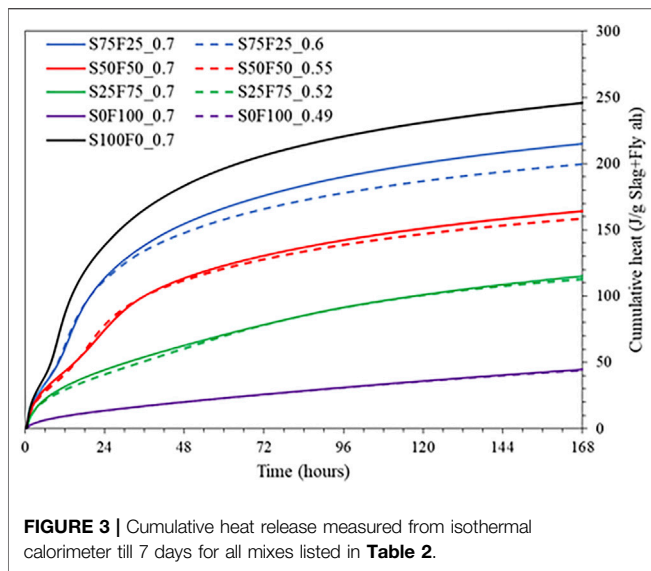
RESULTS AND DISCUSSION

Heat Release From Isothermal Calorimetry

Figure 2 compares the heat release measured from isothermal calorimetry for all the mixes. As previously reported, hydration of NaOH activated slag results in the main peak between 1 and 24 h while sodium silicate-activated slag exhibits a relatively long induction period and the main reaction peak only after 2 days (Shi and Day, 1995; Haha et al., 2011; Haha et al., 2012). Nevertheless, similar cumulative heat of hydration is achieved in both cases. In our case, where the slag is activated with a mixture of NaOH and sodium silicate solution, the main hydration peak is observed after 5 h. Hubler et al. (2011) attributed this main peak to be derived from nucleation and growth of C-S-H based on nucleation seeding experiments.

With a decrease in the amount of slag and an increase in the amount of fly ash in the mixes, we observe a later occurrence of the main hydration peak with a lower intensity. In other words, relatively shorter induction periods and narrower peaks are observed with increasing slag content. This is attributed to the higher reactivity of slag over fly ash, particularly to the fast reaction of the very fine slag particles during early hours, which increases silicate concentration and thereby supersaturation with respect to C-S-H (Gruskovnjak et al., 2006). An increase in the induction period with the addition of fly ash is often reported for Portland cement and C$_3$S (Deschner et al., 2012; Joseph et al., 2017b; Schöler et al., 2017). Mixes with 25% slag (S25F75_0.7 and S25F75_0.52) and without slag (S0F100_0.7 and S0F100_0.52) do not show a distinctive peak within 7 days. The lower heat release with a broader peak and the longer exothermal activity imply slower hydration of the slag-fly ash mixes leading to a lower early-age compressive strength (c.f. *Compressive Strength* section).

An interesting finding is the earlier occurrence of the main peak of hydration at lower solution-to-binder ratios. A slight decrease in the induction period and a faster occurrence of the main peak of alite hydration are often reported for Portland cement and C$_3$S systems at low W/C ratios (Thomas, 2007; Hu et al., 2014; Joseph et al., 2017a). The faster occurrence of the main hydration peak in our samples with slag and fly ash may be due to the variations of alkali concentrations in the solution. We explain this based on two assumptions:

FIGURE 3 | Cumulative heat release measured from isothermal calorimeter till 7 days for all mixes listed in **Table 2**.

1) With the progress of the reaction, there is more consumption of silicate ions compared to OH⁻ ions from the alkali solution;
2) The degree of reaction and microstructure formation for mixes at different S/B ratios are identical till the acceleration period;

It is known that the increase in pH of the pore solution accelerates the occurrence of the main hydration peak (Altan and Erdoğan, 2012; Gebregziabiher et al., 2015) due to the increased dissolution of slag and fly ash, which is strongly dependent on the pH (Song and Jennings, 1999). Although the initial concentrations are the same with different S/B ratios, there are higher amounts of alkalis (c.f. **Table 2**) and higher water content in the overall system with a higher S/B ratio. Hence, at the same degrees of reaction, the concentration of silicates in the pore solution would be lower for the mix with a lower S/B ratio. In that case, the system's pH would be higher for mixes with a lower S/B ratio as the silicate ions induce lower pH compared to the OH⁻ ions. Nevertheless, further study is required to explore this issue in more detail.

Figure 3 shows the cumulative heat released measured until 7 days of reaction. Mixes with higher amounts of slag exhibit higher heat release as expected, owing to its faster reaction kinetics. The heat release is almost similar with respect to the change in the S/B ratio, although it is slightly higher for mixes with a higher S/B ratio. This difference is more pronounced for mixes with a higher volume of slag than those with a lower volume of slag, which is attributed to the increased consumption of alkalis at higher degrees of reaction and lower amount of alkalis in the initial mix composition at lower S/B ratios (c.f. **Table 2**). Nevertheless, it is remarkable that the deviation is almost negligible for all the mixes at least till 1 day of reaction. It should be noted that the heat release within the initial 45 min of reaction has been omitted in the results because this is the time required from mixing to placing the samples in the calorimeter and the time required for the stabilization.

Bound Water Content From TGA

Figure 4 shows the thermogravimetric data and DTG for all the mixes at a 0.7 S/B ratio after 28 days of reaction. In the hydrated alkali-activated slag (S100F0_0.7), two main hydration products are formed as detected in the TGA data: C-S-H (main weight loss at 50°C–200°C) and hydrotalcite-like phase (weight loss at around 200°C and 400°C), which is in agreement with the previous findings (Wang and Scrivener, 2003; Gruskovnjak et al., 2006; Haha et al., 2011). The mass loss from C-S-H consists of the water chemically bound to the structure of C-S-H and physically bound water (Köster and Odler, 1986). The broad peak of hydrotalcite at around 400°C remains almost the same in systems blended with fly ash up to 50%. Increasing fly ash contents beyond this ratio, this hydrotalcite peak becomes weaker. The C-S-H formed from slag hydration is characterized by a higher crystallinity, low Ca/Si ratios, and generally higher aluminum incorporation than that formed in OPC or blended OPC systems (Schneider et al., 2001; Wang and Scrivener, 2003; Gruskovnjak et al., 2006).

From the DTG data, it is noticeable that irrespective of the proportion of slag and fly ash, the profile of the rate of mass loss is similar. While more C-(A)-S-H type reactants are expected from calcium-rich slag-based systems, N-(A)-S-H type reactants are expected to form in low calcium fly ash-based systems (Garcia-Lodeiro et al., 2011). Previous studies also suggest that the dehydroxylation temperature of these C-S-H type gels occurs at similar temperatures (Winnefeld et al., 2010; Ismail et al., 2014). The peak of weight loss in activated fly ash without slag (S0F100_0.7) occurs at around 100°C and is much broader than the one reported by Winnefeld et al. (2010), who attributed this peak to sodium aluminosilicate hydrates. Incorporating the slag and increasing its content, this peak becomes much sharper.

Figure 5 shows the thermogravimetric (TG) data and the first derivative of TG (DTG) for S50F50_0.55 mix after 3, 7, 28, and 90 days of curing. Total mass loss is consistently increasing with an increase in age as expected. Most mass loss occurs before 500°C, indicating a C-(A)-S-H type reaction product (Sakulich et al., 2010). The nature of the peaks does not change over the course of the reaction, and they follow the same trend. As reported previously, alkali-activated slag-fly ash blends can demonstrate the co-existence of the C-A-S-H type gel and geopolymer gel (N-A-S-H) (Wang and Scrivener, 1995; Brough and Atkinson, 2002; Ben Haha et al., 2011; Ismail et al., 2014). The lack of a peak around 600°C–800°C confirms no significant degradation in the samples due to carbonation (Lothenbach et al., 2016).

Figure 6 shows the total bound water content measured from TGA, corresponding to the mass loss between 20°C and 600°C (Lothenbach et al., 2016). With an increasing amount of slag, the bound water content is generally higher because slag exhibits a faster reaction than fly ash. This is noticeable at 3 days when the activated slag (S100F0_0.7) indicates the highest bound water content. However, after 7 days, this situation changes in favor of slag blended with 25% fly ash (S75F25_0.7), showing higher bound water content than activated slag. A striking difference is an increase in the bound water content with an increase in the S/B ratio. This is expected as there is a high amount of alkalis in

FIGURE 4 | (A) TG and **(B)** DTG plots of mixes with an S/B ratio of 0.7 after 28 days of curing.
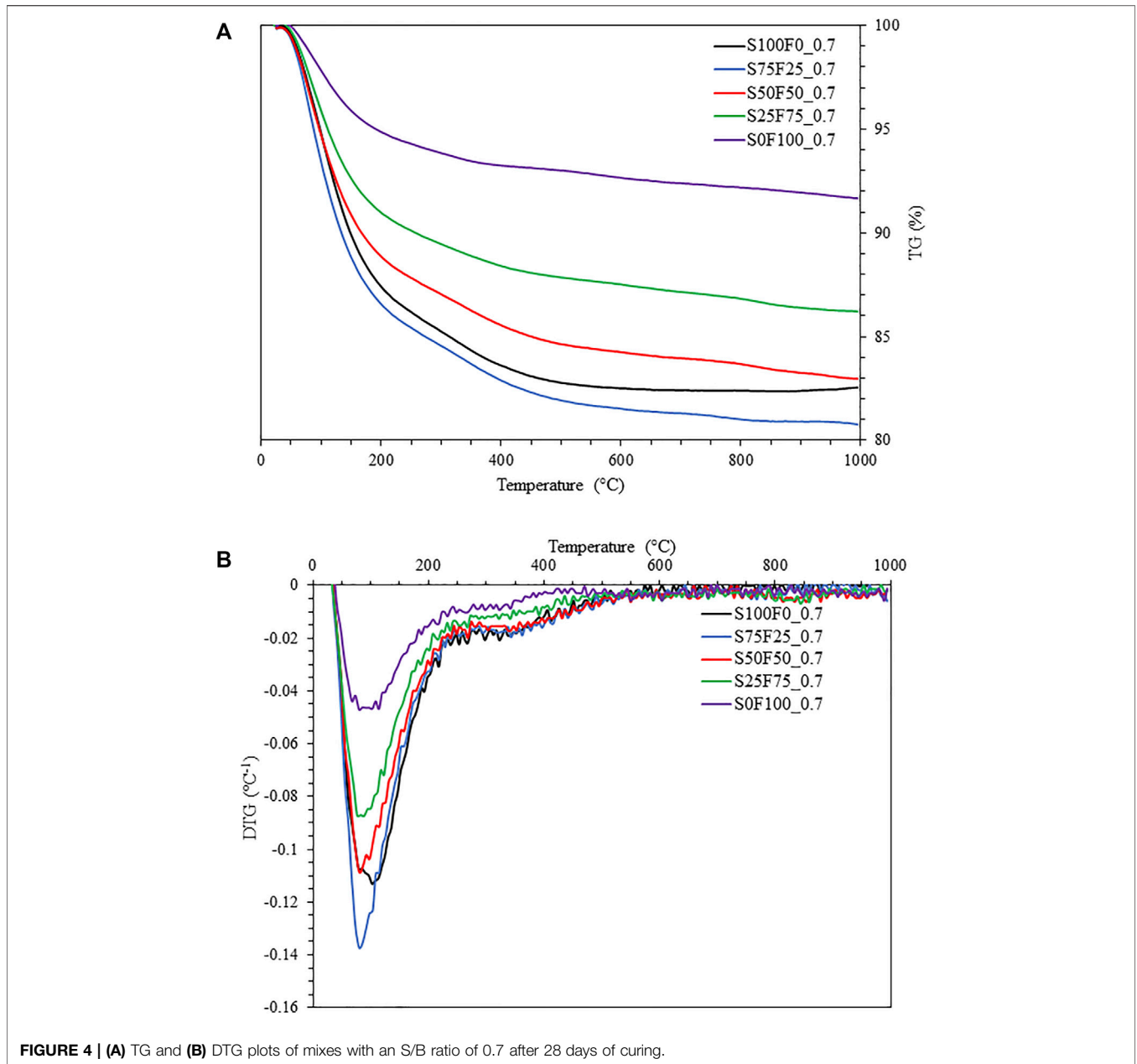
the system (c.f. **Table 2**), which will continue to react with slag and fly ash. This difference is more pronounced at later ages due to the increased consumption of the alkalis.

Compressive Strength

The compressive strength development of the samples listed in **Table 2** is plotted in **Figure 7**. A lower S/B ratio consistently shows higher strengths than the same blends with a higher S/B ratio (Ruiz-Santaquiteria et al., 2012), most likely due to the lower porosity of the system when the S/B ratio is lower. At a similar S/B ratio of 0.7, the strength results are comparable with cumulative heat (**Figure 3**) and bound water content (**Figure 6**), particularly till 7 days.

Regarding the sample S100F0_0.7, the strength does not increase significantly after 7 days. On the one hand, an increase in the bound water content is recorded until 90 days. This seems to be due to microcracking induced by shrinkage that can cause a strength loss (Collins and Sanjayan, 2001; Wardhono et al., 2015). On the other hand, there is a continuous increase in the strength of the other samples. In the early ages (3 and 7 days), samples with a higher proportion of blast furnace slag yield a higher strength which could be attributed to the higher reactivity of slag over fly ash. At 28 days, for the same S/B ratio of 0.7, the compressive strengths of S100F0_0.7, S75F25_0.7, and S50F50_0.7 are almost similar. Considering the samples with a similar flow, by 28 and 90 days, the samples with 25% and 50%

FIGURE 5 | (A) TG and **(B)** DTG plots of S50F50_0.55 at 3, 7, 28, and 90 days.
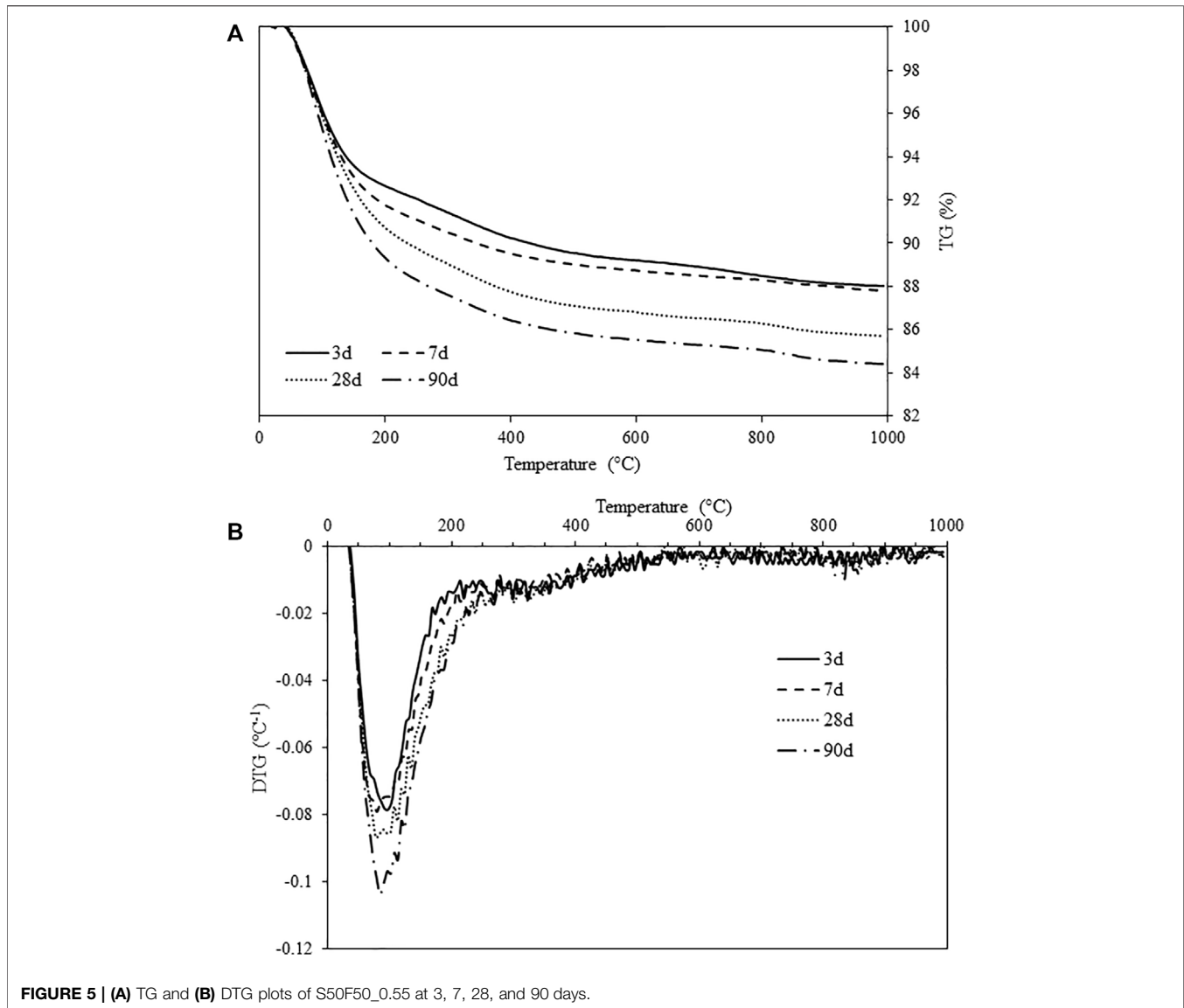
slag replacement with fly ash (S75F25_0.6 and S50F50_0.55, respectively) have higher strength values than the one with 100% slag (S100F0_0.7). Compared to Portland cement, while the strength of 25% slag (S25F75_0.52) after 28 days is in the same range with CEM I 52.5 with a 0.5 W/C ratio, samples with higher percentages of slag are much superior even at higher S/B ratios. There are no surprises here as similar results are often reported in the literature (Puertas et al., 2000; Nath and Sarker, 2014; Fang et al., 2018).

Bound Water Content *Versus* Heat Release

Figure 8 compares the overall cumulative heat released per gram of binder measured from isothermal calorimetry with the bound water content measured from TGA after 3 and 7 days of curing. A good correlation exists with an R^2 value of 0.97. The comparison could only be drawn until 7 days due to the lack of calorimetry data beyond 7 days. A remarkable outcome of this correlation is

that irrespective of the amount of slag and fly ash in the current systems, the bound water content and heat release is proportional to each other, both being a good indication for hydrate formation. Nevertheless, there is an offset for the trend line amounting to around 56 J. Part of this could be due to the omission of heat release in the first 45 min. This needs to be addressed in detail in future studies by comparing the early age heat release with TGA (<3 days).

Compressive Strength *Versus* Bound Water Content

Figure 9 compares the compressive strength with the bound water content determined from TGA. While the general trend can be captured, the correlation is slightly poor, with an R^2 value of less than 0.7, due to the different S/B ratios that lead to differences in initial porosity. This is evident from **Figure 6** and **Figure 7**, as a
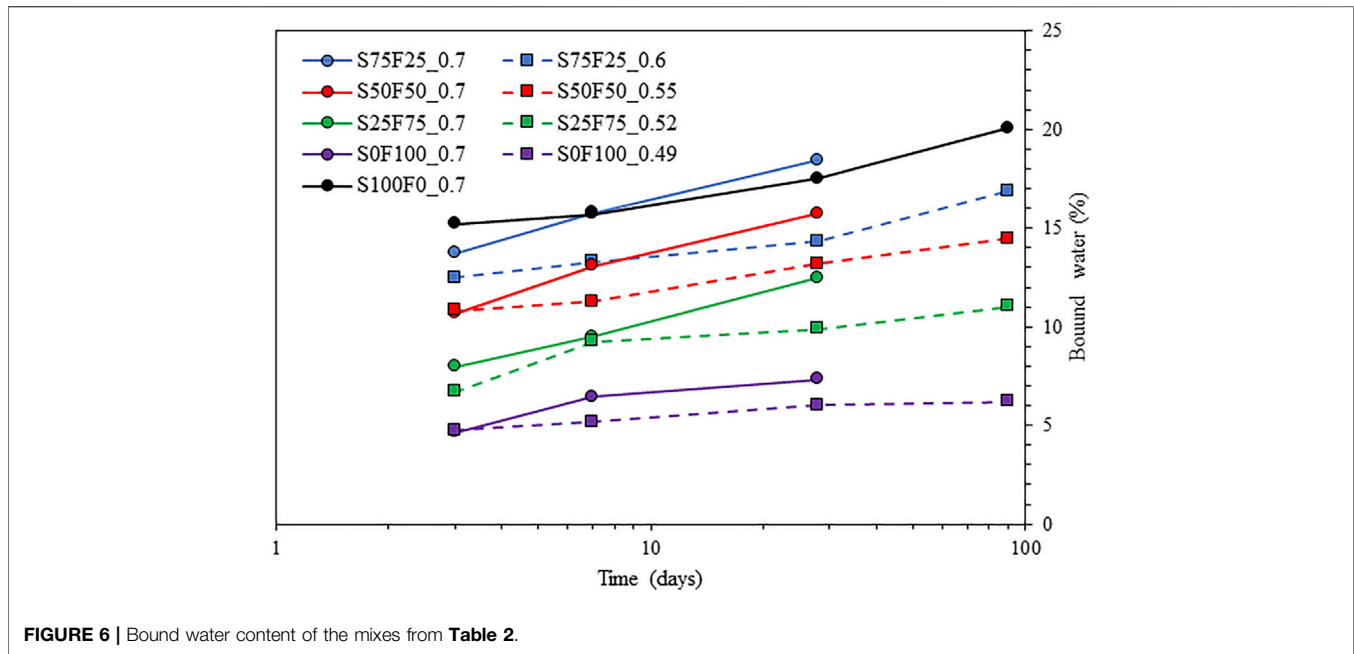
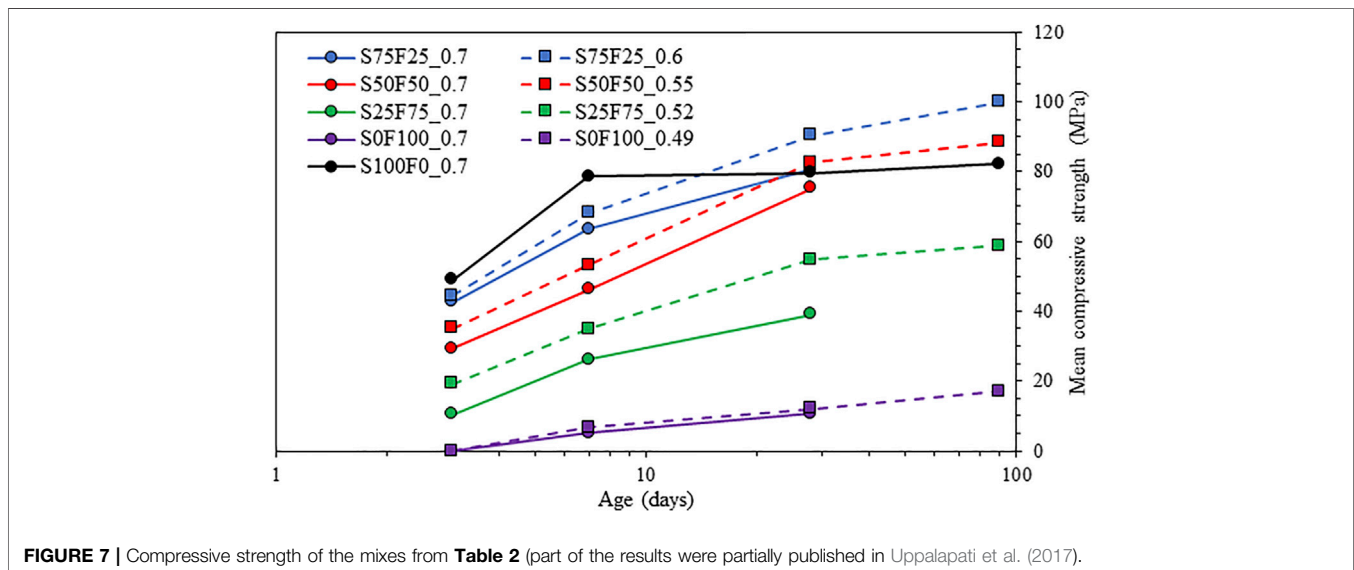**FIGURE 6 |** Bound water content of the mixes from **Table 2**.

FIGURE 7 | Compressive strength of the mixes from **Table 2** (part of the results were partially published in Uppalapati et al. (2017).

lower S/B ratio leads to a higher compressive strength but a lower bound water content. Hence, the mixes with the same S/B ratio of 0.7 are compared in **Figure 10**, which gives much better correlations (R^2 of ~ 0.9). The outlier S100F0_0.7 after 90 days of reaction is marked in **Figure 10**.
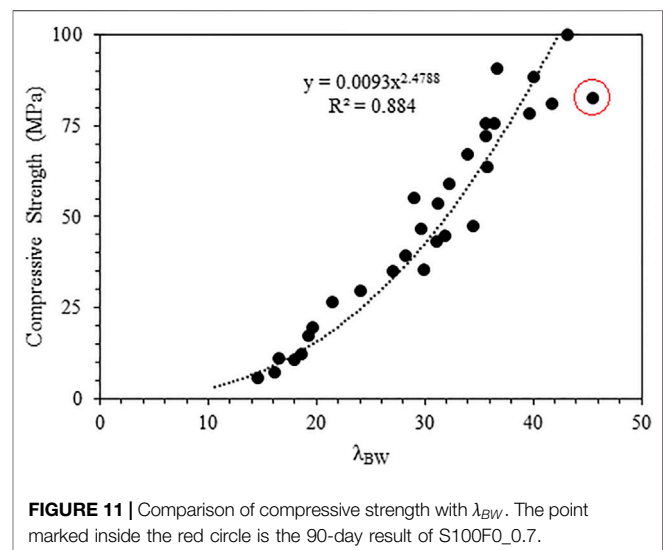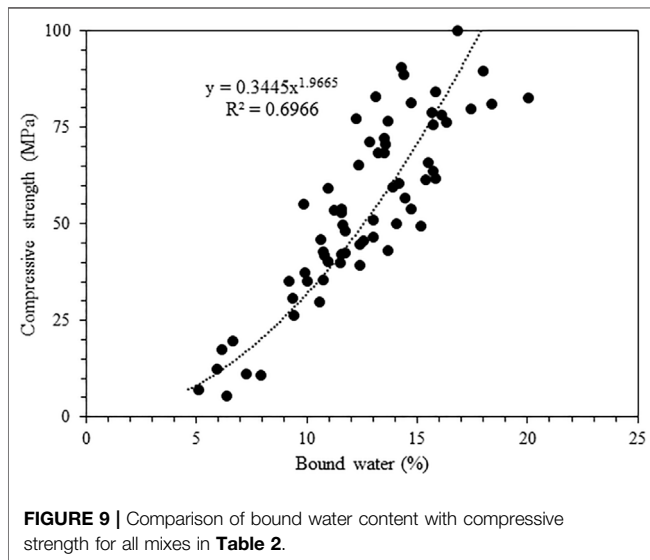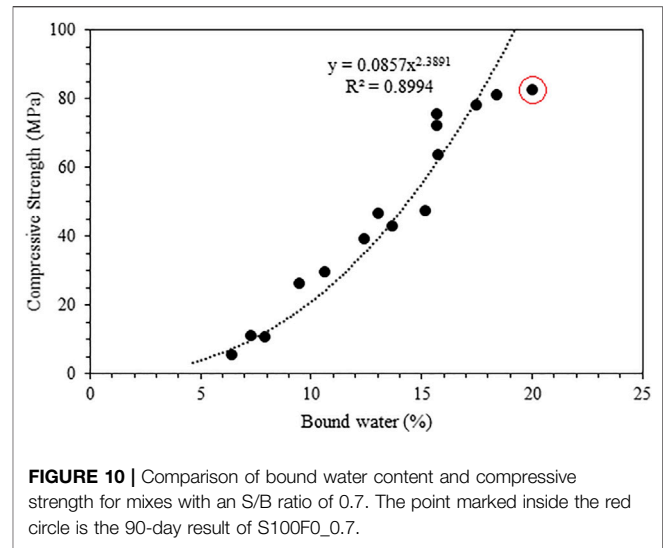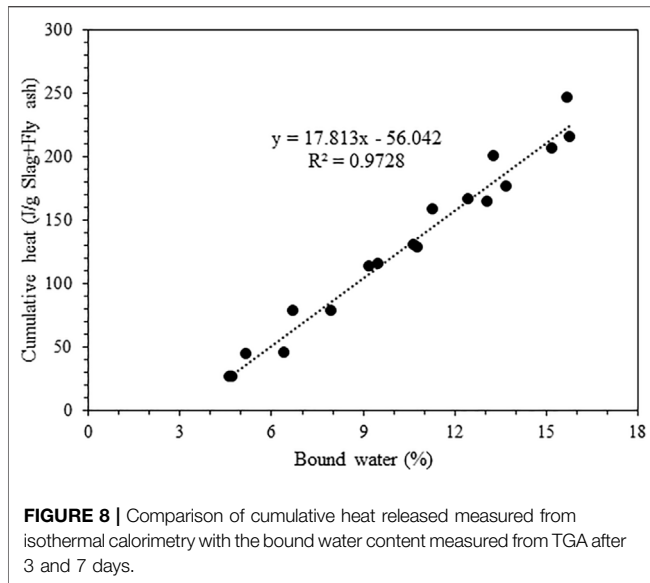
To consider the effect of the porosity while varying the S/B ratio, a new parameter λ_{BW} is introduced. It is defined as follows:

$$\lambda_{BW} = BW/Ws, \qquad (1)$$

where BW is the bound water content in percentage and Ws is the water-to-solid ratio (W/S). The rationale behind selecting such a parameter is that this could consider the effect of initial porosity

to a certain extent. A higher W/S ratio will contribute to a decrease in strength and vice versa. Such a parameter could mimic Schiller's model (Schiller et al., 1971), where the increase in strength is correlated with the decrease in capillary porosity and initial porosity. An increase in bound water content corresponds to the hydrate formation and thereby reduction in total porosity.

A significant improvement in the correlation with an R^2 of 0.88 is obtained when compressive strength is compared with λ_{BW} (**Figure 11**). While the number of hydration products and the amount of initial porosity are important parameters for strength development, other parameters could explain the

FIGURE 8 | Comparison of cumulative heat released measured from isothermal calorimetry with the bound water content measured from TGA after 3 and 7 days.

FIGURE 10 | Comparison of bound water content and compressive strength for mixes with an S/B ratio of 0.7. The point marked inside the red circle is the 90-day result of S100F0_0.7.

FIGURE 9 | Comparison of bound water content with compressive strength for all mixes in **Table 2**.

FIGURE 11 | Comparison of compressive strength with λ_{BW}. The point marked inside the red circle is the 90-day result of S100F0_0.7.

recorded deviations. One of the major ones can be the microcracking of samples at later ages due to shrinkage, particularly for the mix with 100% slag, as indicated in the previous section. The result of the 90-day strength of S100F0_0.7, which is highlighted with a red circle in **Figure 10** and **Figure 11**, is the most deviated one from the trend lines. Nevertheless, no visible cracks were observed on these samples, assuming there were microcracks. Furthermore, other parameters are not included in this approach, including pore structure (Kumar and Bhattacharjee, 2003; Chindaprasirt et al., 2005) and interfacial transition zone (Ollivier et al., 1995).

TGA is costly equipment, so an alternative route using an oven could be considered. The mass loss could be calculated for samples after arresting the reaction from a laboratory oven by keeping the sample at 600°C by taking the mass before and after
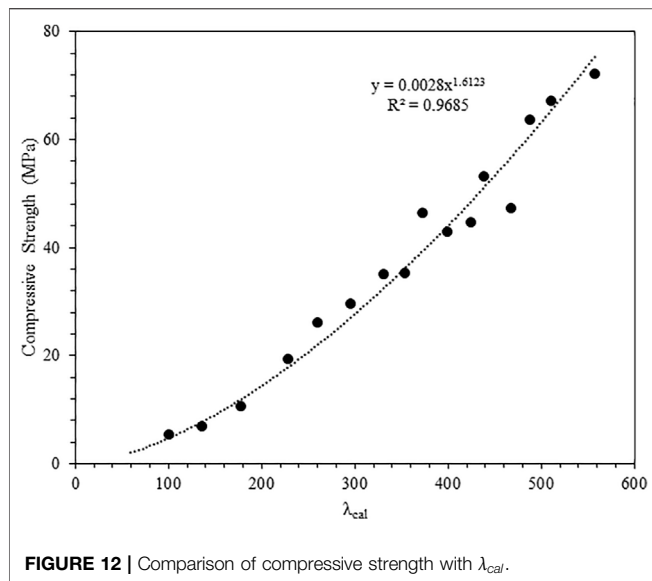
placing it in the oven. Precautions need to be made with respect to the holding time, as the temperature displayed in the oven may not be the temperature of the material. Furthermore, there could be errors in measurements due to oxidation at high temperatures if an inert gas such as N_2 is not used (Bernal et al., 2017).

Compressive Strength *Versus* Heat Release

This section compares the compressive strength with heat release from calorimetry till 7 days. Similar to the approach used in the previous section, to consider the effect of the S/B ratio, the parameter λ_{cal} is introduced:

$$\lambda_{cal} = Q/Ws, \qquad (2)$$

where Q is the cumulative heat released measured from the isothermal calorimeter and *Ws* is the water-to-solid ratio (W/S).

FIGURE 12 | Comparison of compressive strength with λ_{cal}.

comprises 50% 5 of 5 M NaOH and 50% of water glass (sodium silicate solution).

The major conclusions of this study are as follows:

1) At similar S/B ratios, mixes with higher amounts of slag have higher compressive strength and bound water content till 28 days and higher heat release till 7 days.
2) Comparing mixes with similar flow and varying S/B ratios, fly ash replacement up to 50% has a higher strength than the mix with 100% slag. This is due to the ball-bearing effect of fly ash, which reduces the water demand to achieve similar workability.
3) The S/B ratio hardly affects the cumulative heat released till 1 day of reaction. On the contrary, there is a considerable increase in the bound water content with an increase in S/B, particularly at later ages.
4) A good linear correlation is obtained between bound water content and heat release measured from the calorimeter.
5) Compressive strength correlates well with cumulative heat release and bound water content when the water-to-solid ratio of the initial mixture is also considered.

Figure 12 shows a good correlation between the compressive strength and λ_{cal} (R^2 = 0.97). This is expected as a good linear correlation exists between the bound water content and the cumulative heat release (**Figure 8**). A higher R^2 for **Figure 12** compared to **Figure 11** shall not be interpreted as this approach is better than bound water content because, in this case, only measurements until 7 days are compared.

DATA AVAILABILITY STATEMENT

The original contributions presented in the study are included in the article/Supplementary Material, further inquiries can be directed to the corresponding author.

CONCLUSION

This work studies different blends of alkali-activated slag and fly ash with isothermal calorimetry, thermogravimetric analysis, and compressive strength to understand the correlations between them. Ground granulated blast furnace slag and coal combustion fly ash at different proportions (100:0, 75:25, 50:50, 25:75, and 0:100) are used with two different solution-to-binder (S/B) ratios. A constant S/B ratio of 0.7 and a varied S/B ratio, which give similar mortar flow, were used. Alkali solution

AUTHOR CONTRIBUTIONS

SJ conducted the experiments, analysed the data, prepared the figures, and wrote the manuscript. ÖC acquired funding, supervised the study, and edited the manuscript.

REFERENCES

Altan, E., and Erdoğan, S. T. (2012). Alkali Activation of a Slag at Ambient and Elevated Temperatures. *Cem. Concr. Compos.* 34, 131–139. doi:10.1016/j.cemconcomp.2011.08.003

Ben Haha, M., Le Saout, G., Winnefeld, F., and Lothenbach, B. (2011). Influence of Activator Type on Hydration Kinetics, Hydrate Assemblage and Microstructural Development of Alkali Activated Blast-Furnace Slags. *Cem. Concr. Res.* 41, 301–310. doi:10.1016/j.cemconres.2010.11.016

Bernal, S. A. (2016). Advances in Nearneutral Salts Activation of Blast Furnace Slags. *RILEM Tech. Lett.* 1, 3944. doi:10.21809/rilemtechlett.2016.8

Bernal, S. A., Juenger, M. C. G., Ke, X., Matthes, W., Lothenbach, B., De Belie, N., et al. (2017). Characterization of Supplementary Cementitious Materials by thermal Analysis. *Mater. Struct. Constr.* 50, 1–13. doi:10.1617/s11527-016-0909-2

Brough, A. R., and Atkinson, A. (2002). Sodium Silicate-Based, Alkali-Activated Slag Mortars - Part I. Strength, Hydration and Microstructure. *Cem. Concr. Res.* 32, 865–879. doi:10.1016/S0008-8846(02)00717-2

Chindaprasirt, P., Jaturapitakkul, C., and Sinsiri, T. (2005). Effect of Fly Ash Fineness on Compressive Strength and Pore Size of Blended Cement Paste. *Cem. Concr. Compos.* 27, 425–428. doi:10.1016/j.cemconcomp.2004.07.003

Collins, F., and Sanjayan, J. G. (2001). Microcracking and Strength Development of Alkali Activated Slag concrete. *Cem. Concr. Compos.* 23, 345–352. doi:10.1016/S0958-9465(01)00003-8

Deschner, F., Winnefeld, F., Lothenbach, B., Seufert, S., Schwesig, P., Dittrich, S., et al. (2012). Hydration of Portland Cement with High Replacement by Siliceous Fly Ash. *Cem. Concr. Res.* 42, 1389–1400. doi:10.1016/j.cemconres.2012.06.009

Fang, G., Ho, W. K., Tu, W., and Zhang, M. (2018). Workability and Mechanical Properties of Alkali-Activated Fly Ash-Slag concrete Cured at Ambient Temperature. *Constr. Build. Mater.* 172, 476–487. doi:10.1016/j.conbuildmat.2018.04.008

Fei, J., Kai, G., Adel, A., and Abir, A.-T. (2015). Effects of Different Reactive MgOs on the Hydration of MgO-Activated GGBS Paste. *J. Mater. Civ. Eng.* 27, B4014001. 1943-5533.0001009. doi:10.1061/(ASCE)MT

Garcia-Lodeiro, I., Palomo, A., Fernández-Jiménez, A., and MacPhee, D. E. (2011). Compatibility Studies between N-A-S-H and C-A-S-H Gels. Study in the Ternary Diagram Na2O-CaO-Al2O3-SiO 2-H2O. *Cem. Concr. Res.* 41, 923–931. doi:10.1016/j.cemconres.2011.05.006

Gebregziabiher, B. S., Thomas, R., and Peethamparan, S. (2015). Very Early-Age Reaction Kinetics and Microstructural Development in Alkali-Activated Slag. *Cem. Concr. Compos.* 55, 91–102. doi:10.1016/j.cemconcomp.2014.09.001

Gong, K., and White, C. E. (2016). Impact of Chemical Variability of Ground Granulated Blast-Furnace Slag on the Phase Formation in Alkali-Activated Slag Pastes. *Cem. Concr. Res.* 89, 310–319. doi:10.1016/j.cemconres.2016.09.003

Gruskovnjak, A., Lothenbach, B., Holzer, L., Figi, R., and Winnefeld, F. (2006). Hydration of Alkali-Activated Slag: Comparison with Ordinary Portland Cement. *Adv. Cem. Res.* 18, 119–128. doi:10.1680/adcr.2006.18.3.119

Haha, M., Lothenbach, B., Le Saout, G., and Winnefeld, F. (2011). Influence of Slag Chemistry on the Hydration of Alkali-Activated Blast-Furnace Slag - Part I: Effect of MgO. *Cem. Concr. Res.* 41, 955–963. doi:10.1016/j.cemconres.2011.05.002

Haha, M., Lothenbach, B., Le Saout, G., and Winnefeld, F. (2012). Influence of Slag Chemistry on the Hydration of Alkali-Activated Blast-Furnace Slag - Part II: Effect of Al2O3. *Cem. Concr. Res.* 42, 74–83. doi:10.1016/j.cemconres.2011.08.005

Hu, J., Ge, Z., and Wang, K. (2014). Influence of Cement Fineness and Water-To-Cement Ratio on Mortar Early-Age Heat of Hydration and Set Times. *Constr. Build. Mater.* 50, 657–663. doi:10.1016/j.conbuildmat.2013.10.011

Hubler, M. H., Thomas, J. J., and Jennings, H. M. (2011). Influence of Nucleation Seeding on the Hydration Kinetics and Compressive Strength of Alkali Activated Slag Paste. *Cem. Concr. Res.* 41, 842–846. doi:10.1016/j.cemconres.2011.04.002

Ismail, I., Bernal, S. A., Provis, J. L., San Nicolas, R., Hamdan, S., and Van Deventer, J. S. J. (2014). Modification of Phase Evolution in Alkali-Activated Blast Furnace Slag by the Incorporation of Fly Ash. *Cem. Concr. Compos.* 45, 125–135. doi:10.1016/j.cemconcomp.2013.09.006

Jin, F., Gu, K., and Al-Tabbaa, A. (2014). Strength and Drying Shrinkage of Reactive MgO Modified Alkali-Activated Slag Paste. *Constr. Build. Mater.* 51, 395–404. doi:10.1016/j.conbuildmat.2013.10.081

Jin, Y., and Stephan, D. (2019). The Unusual Solidification Process of Alkali Activated Slag and its Relationship with the Glass Structure of the Slag. *Cem. Concr. Res.* 121, 1–10. doi:10.1016/j.cemconres.2019.04.004

Joseph, S., Bishnoi, S., Van Balen, K., and Cizer, O. (2017a). Effect of the Densification of C-S-H on Hydration Kinetics of Tricalcium Silicate. *J. Am. Ceram. Soc.* 101 (6), 2438–2449. doi:10.1111/jace.15390

Joseph, S., Bishnoi, S., Van Balen, K., and Cizer, Ö. (2017b). Modeling the Effect of Fineness and Filler in Early-Age Hydration of Tricalcium Silicate. *J. Am. Ceram. Soc.* 100, 1178–1194. doi:10.1111/jace.14676

Joseph, S., and Cizer, O. (2020). Effect of Grinding on the Quantification of Bound Water in Tricalcium Silicate. *Adv. Cem. Res.* 32, 476–480. doi:10.1680/jadcr.18.00199

Juenger, M. C. G., Winnefeld, F., Provis, J. L., and Ideker, J. H. (2011). Advances in Alternative Cementitious Binders. *Cem. Concr. Res.* 41, 1232–1243. doi:10.1016/j.cemconres.2010.11.012

Köster, H., and Odler, I. (1986). Investigations on the Structure of Fully Hydrated portland Cement and Tricalcium Silicate Pastes. I. Bound Water, Chemical Shrinkage and Density of Hydrates. *Cem. Concr. Res.* 16, 207–214. doi:10.1016/0008-8846(86)90137-7

Kumar, R., and Bhattacharjee, B. (2003). Porosity, Pore Size Distribution and *In Situ* Strength of concrete. *Cem. Concr. Res.* 33, 155–164. doi:10.1016/S0008-8846(02)00942-0

Kumar, S., Kumar, R., and Mehrotra, S. P. (2010). Influence of Granulated Blast Furnace Slag on the Reaction, Structure and Properties of Fly Ash Based Geopolymer. *J. Mater. Sci.* 45, 607–615. doi:10.1007/s10853-009-3934-5

Kutchko, B. G., and Kim, A. G. (2006). Fly Ash Characterization by SEM-EDS. *Fuel* 85, 2537–2544. doi:10.1016/j.fuel.2006.05.016

Li, X., Snellings, R., Antoni, M., Mariel, N., Cyr, M., Ben, M., et al. (2018). Reactivity Tests for Supplementary Cementitious Materials : RILEM TC 267-TRM Phase 1. 0123456789. doi:10.1617/s11527-018-1269-x

Lothenbach, B., Durdzinski, P., and De Weerdt, K. (2016). "Thermogravimetric Analysis," in *A Practical Guide to Microstructural Analysis of Cementitious Materials*. Editors K. L. Scrivener, R. Snellings, and B. Lothenbach (CRC Press), 177–212.

Luukkonen, T., Heponiemi, A., Runtti, H., Pesonen, J., Yliniemi, J., and Lassi, U. (2019). Application of Alkali-Activated Materials for Water and Wastewater Treatment: a Review. *Rev. Environ. Sci. Biotechnol.* 18, 271–297. doi:10.1007/s11157-019-09494-0

Marjanović, N., Komljenović, M., Baščarević, Z., Nikolić, V., and Petrović, R. (2015). Physical-mechanical and Microstructural Properties of Alkali-Activated Fly Ash-Blast Furnace Slag Blends. *Ceram. Int.* 41, 1421–1435. doi:10.1016/j.ceramint.2014.09.075

Mutti, M., Joseph, S., and Cizer, O. (2020). "Sodium Sulfate and Sodium Hydroxide Co-activation of Blast Furnace Slag," in B. Abstr. 74 th RILEM Annu. Week 40 th Cem. Concr. Sci. Conf.

Nath, P., and Sarker, P. K. (2014). Effect of GGBFS on Setting, Workability and Early Strength Properties of Fly Ash Geopolymer concrete Cured in Ambient Condition. *Constr. Build. Mater.* 66, 163–171. doi:10.1016/j.conbuildmat.2014.05.080

Ollivier, J. P., Maso, J. C., and Bourdette, B. (1995). Interfacial Transition Zone in concrete. *Adv. Cem. Based Mater.* 2, 30–38. doi:10.1016/1065-7355(95)90037-3

Pachego-Torgal, F., Labrincha, J., Leonelli, C., Palomo, A., and Chindaprasit, P. (2015). *Handbook of Alkali-Activated Cements, Mortars and Concretes*. Woodhead Publishing.

Provis, J., and Deventer, J. (2014). Alkali Activated Materials: State-Of-The-Art Report. *RILEM TC 224-AAM*, 459–491. doi:10.1007/978-94-007-7672-2

Provis, J. L. (2018). Alkali-activated Materials. *Cem. Concr. Res.* 114, 40–48. doi:10.1016/j.cemconres.2017.02.009

Provis, J. L., and Bernal, S. A. (2014). Geopolymers and Related Alkali-Activated Materials. *Annu. Rev. Mater. Res.* 44, 299–327. doi:10.1146/annurev-matsci-070813-113515

Puertas, F., Martínez-Ramírez, S., Alonso, S., and Vázquez, T. (2000). Alkali-activated Fly Ash/slag Cements. Strength Behaviour and Hydration Products. *Cem. Concr. Res.* 30, 1625–1632. doi:10.1016/S0008-8846(00)00298-2

Puligilla, S., and Mondal, P. (2013). Role of Slag in Microstructural Development and Hardening of Fly Ash-Slag Geopolymer. *Cem. Concr. Res.* 43, 70–80. doi:10.1016/j.cemconres.2012.10.004

Rashad, A. M., Bai, Y., Basheer, P. A. M., Milestone, N. B., and Collier, N. C. (2013). Hydration and Properties of Sodium Sulfate Activated Slag. *Cem. Concr. Compos.* 37, 20–29. doi:10.1016/j.cemconcomp.2012.12.010

Roy, D. M. (1999). Alkali Activated Cements, Opportunities and Challenges. *Cem. Concr. Res.* 29, 249–254. doi:10.1016/s0008-8846(98)00093-3

Ruiz-Santaquiteria, C., Skibsted, J., Fernández-Jiménez, A., and Palomo, A. (2012). Alkaline Solution/binder Ratio as a Determining Factor in the Alkaline Activation of Aluminosilicates. *Cem. Concr. Res.* 42, 1242–1251. doi:10.1016/j.cemconres.2012.05.019

Sakulich, A. R., Miller, S., and Barsoum, M. W. (2010). Chemical and Microstructural Characterization of 20-Month-Old Alkali-Activated Slag Cements. *J. Am. Ceram. Soc.* 93, 1741–1748. doi:10.1111/j.1551-2916.2010.03611.x

Schiller, K. K., Phil, D., and Inst, P. F. (1971). Strength of Porous Materials. *Cem. Concr. Res.* 1, 419–422. doi:10.1016/0008-8846(71)90035-4

Schneider, J., Cincotto, M. A., and Panepucci, H. (2001). 29Si and 27Al High-Resolution NMR Characterization of Calcium Silicate Hydrate Phases in Activated Blast-Furnace Slag Pastes. *Cem. Concr. Res.* 31, 993–1001. doi:10.1016/S0008-8846(01)00530-0

Schöler, A., Lothenbach, B., Winnefeld, F., Haha, M., Zajac, M., and Ludwig, H. M. (2017). Early Hydration of SCM-Blended Portland Cements: A Pore Solution and Isothermal Calorimetry Study. *Cem. Concr. Res.* 93, 71–82. doi:10.1016/j.cemconres.2016.11.013

Scrivener, K. L., John, V. M., and Gartner, E. M. (2018). Eco-efficient Cements: Potential Economically Viable Solutions for a low-CO2 Cement-Based Materials Industry. *Cem. Concr. Res.* 114, 2–26. doi:10.1016/j.cemconres.2018.03.015

Shi, C., and Day, R. L. (1995). A Calorimetric Study of Early Hydration of alkali.Pdf. *Cem. Concr. Res.* 25, 1333–1346. doi:10.1016/0008-8846(95)00126-w

Skibsted, J., and Snellings, R. (2019). Reactivity of Supplementary Cementitious Materials (SCMs) in Cement Blends. *Cem. Concr. Res.* 124. doi:10.1016/j.cemconres.2019.105799

Snellings, R. (2016). Assessing, Understanding and Unlocking Supplementary Cementitious Materials. *RILEM Tech. Lett.* 1, 50. doi:10.21809/rilemtechlett.2016.12

Song, S., and Jennings, H. M. (1999). Pore Solution Chemistry of Alkali-Activated Ground Granulated Blast-Furnace Slag. *Cem. Concr. Res.* 29, 159–170. doi:10.1016/S0008-8846(98)00212-9

Suraneni, P., Hajibabaee, A., Ramanathan, S., Wang, Y., and Weiss, J. (2019). New Insights from Reactivity Testing of Supplementary Cementitious Materials. *Cem. Concr. Compos.* 103, 331–338. doi:10.1016/j.cemconcomp.2019.05.017

Thomas, J. J. (2007). A New Approach to Modeling the Nucleation and Growth Kinetics of Tricalcium Silicate Hydration. *J. Am. Ceram. Soc.* 90, 3282–3288. doi:10.1111/j.1551-2916.2007.01858.x

Uppalapati, S., Joseph, S., and Cizer, Ö. (2017). Autogenous Shrinkage and Strength Development of Alkali-Activated Slag/Fly Ash Mortar Blends.

Wang, S. D., and Scrivener, K. L. (2003). 29Si and 27Al NMR Study of Alkali-Activated Slag. *Cem. Concr. Res.* 33, 769–774. doi:10.1016/S0008-8846(02)01044-X

Wang, S. D., and Scrivener, K. L. (1995). Hydration Products of Alkali Activated Slag Cement. *Cem. Concr. Res.* 25, 561–571. doi:10.1016/0008-8846(95)00045-E

Wang, S. D., Scrivener, K. L., and Pratt, P. L. (1994). Factors Affecting the Strength of Alkali-Activated Slag. *Cem. Concr. Res.* 24, 1033–1043. doi:10.1016/0008-8846(94)90026-4

Wardhono, A., Law, D. W., and Strano, A. (2015). The Strength of Alkali-Activated Slag/fly Ash Mortar Blends at Ambient Temperature. *Proced. Eng.* 125, 650–656. doi:10.1016/j.proeng.2015.11.095

Winnefeld, F., Leemann, A., Lucuk, M., Svoboda, P., and Neuroth, M. (2010). Assessment of Phase Formation in Alkali Activated Low and High Calcium Fly Ashes in Building Materials. *Constr. Build. Mater.* 24, 1086–1093. doi:10.1016/j.conbuildmat.2009.11.007